Theory of perturbative pulse train based coherent control

Cite as: J. Chem. Phys. **140**, 124307 (2014); https://doi.org/10.1063/1.4869080
Submitted: 16 December 2013 • Accepted: 10 March 2014 • Published Online: 24 March 2014

Timur Grinev and Paul Brumer

Theory of perturbative pulse train based coherent control

Timur Grinev and Paul Brumer
Department of Chemistry, Chemical Physics Theory Group and Center for Quantum Information and Quantum Control, University of Toronto, Toronto, Ontario M5S 3H6, Canada

(Received 16 December 2013; accepted 10 March 2014; published online 24 March 2014)

A theoretical description of coherent control of excited state dynamics using pulse trains in the perturbative regime, as carried out in recent experiments, is presented. Analytical expressions relating the excited state populations to the pulse train control parameters are derived. Numerical examples are provided for models of pyrazine and β-carotene, and the significant role of overlapping resonances is exposed. © *2014 AIP Publishing LLC*. [http://dx.doi.org/10.1063/1.4869080]

I. INTRODUCTION

Coherent control[1] uses molecular interference terms, manipulated by varying various laboratory control parameters, to control molecular dynamics. Within this framework, a number of recent experimental studies[2–4] considered the use of pulse trains to control excited state populations. In this case a shaped pulse train is used to affect population dynamics, which are measured using pump-DFWM (degenerate four-wave mixing) techniques. These experiments, which operate in the perturbative regime, were accompanied by numerical simulations[2,3,5] intended to investigate the control mechanism. However, the influence of pulse control parameters on excited state population dynamics, and their relation to fundamental issues such as overlapping resonances[6–8] was not clearly elucidated.

It should be remarked at the outset that the pump-DFWM experiments fall into the class of nonlinear spectroscopy whose outcome is expected to depend on the temporal profile of the pulses. Here, however, we present a simple analytical description of the excited state population dynamics in such studies, which give useful analytical insight, display the influence of the laser pulse parameters on the controlled excited state population, and provide the relationship of control to molecular properties such as overlapping resonances. Further, we utilize a generic (projection operator) approach to the measurement process that follows the dynamics that are induced by the pump step. In this way we can readily expose the relationship between the controlled dynamics and the molecular properties without involving details of the measurement.

The paper is organized as follows: Section II presents the theory of Gaussian based pulse train driven excitation. Numerical examples are then given in Sec. III, followed by a summary in Sec. IV. The latter also clarifies the relation of this pulse train control to the issue of one-photon phase control.[9]

II. PULSE TRAIN DRIVEN $S_0 \rightarrow S_2/S_1$ EXCITATION AND $S_2 \leftrightarrow S_1$ INTERCONVERSION

As a generic example, we consider a molecular system having the ground singlet electronic state S_0 and two excited electronic states S_1 and S_2. These excited states are assumed to display a conical intersection, inducing rapid femtosecond $S_2 \leftrightarrow S_1$ internal conversion (IC). Initially, the molecular system is assumed to be in the S_0 state. Subsequent excitation by means of a weak laser field produces the vibronic $S_1 + S_2$ wave packet, whose properties depend on the frequency profile of the excitation laser. Simultaneously, this wave packet evolves on $S_1 + S_2$ due to $S_1 \leftrightarrow S_2$ coupling. Below we consider the pulse train of Refs. 2–4, acting on Hermitian and model non-Hermitian quantum systems. Spontaneous emission, which occurs on longer timescales, is neglected.

A. Gaussian based pulse train

The coherent control pulse train experiments in Refs. 2–4 utilize shaped pulses that are produced as follows. Starting from a transform-limited (TL) Gaussian pulse, its phase Φ_{PM} is modulated in the frequency domain with a sine function, $\Phi_{PM}(\omega) = a \sin(b\omega + c)$, while keeping the amplitude profile intact. The parameters a, b, c are then varied to control molecular populations. The resultant phase-modulated (PM) electric field is given by

$$\begin{aligned}\varepsilon_{PM}(\omega) &= \varepsilon_{TL}(\omega) e^{i\Phi_{PM}(\omega)} = \varepsilon_{TL}(\omega) e^{ia\sin(b\omega+c)} \\ &= \epsilon\, e^{-\alpha^2(\omega-\omega_0)^2} e^{ia\sin(b\omega+c)},\end{aligned} \tag{1}$$

where ω_0 is the center frequency of the pulse, α is the pulse width, and ϵ is the normalization constant. Using the Jacobi-Anger expansion[10] we have

$$e^{ia\sin(b\omega+c)} = \sum_{n=-\infty}^{n=+\infty} J_n(a) e^{in(b\omega+c)}, \tag{2}$$

where $J_n(a)$ is the Bessel function of the first kind.[11] The PM pulse in the time domain, $\varepsilon_{PM}(t)$, is obtained by the inverse Fourier transform of $\varepsilon_{PM}(\omega)$ in Eq. (1),

$$\varepsilon_{PM}(t) = \frac{1}{2\pi} \int_{-\infty}^{+\infty} d\omega\, \varepsilon_{PM}(\omega)\, e^{-i\omega t}, \tag{3}$$

giving

$$\varepsilon_{PM}(t) = \sum_{n=-\infty}^{n=+\infty} J_n(a) e^{inc} \varepsilon_{TL}(t - nb), \tag{4}$$

which is composed of individual TL pulses ε_{TL} at times $t - nb$. Each pulse has a specific phase $nc + \pi(1 - \text{sign}(J_n(a)))/2$ and amplitude proportional to $|J_n(a)|$. In the rotating wave approximation, $\varepsilon_{TL}(t - nb)$ is

$$\varepsilon_{TL}(t - nb) = \frac{\epsilon}{2\sqrt{\pi}\alpha} e^{-\left(\frac{t-nb}{2\alpha}\right)^2 - i\omega_0(t-nb)}. \tag{5}$$

The finite-time Fourier transform of the pulse train in Eq. (4) is

$$\begin{aligned}\varepsilon_{PM}(\omega, t) &\equiv \int_{-\infty}^{t} dt' \varepsilon_{PM}(t') e^{i\omega t'} \\ &= \sum_{n=-\infty}^{n=+\infty} J_n(a) e^{in(b\omega + c)} \varepsilon_{TL}(\omega, t - nb),\end{aligned} \tag{6}$$

where $\varepsilon_{TL}(\omega, t - nb)$ is the finite-time Fourier transform of the TL pulse [Eq. (5)] at time $t - nb$.[12,13] That is,

$$\begin{aligned}\varepsilon_{TL}(\omega, t - nb) = (\epsilon/2) e^{-\alpha^2(\omega-\omega_0)^2} \\ \times \left\{2 - e^{[\beta(\omega, t-nb)]^2} W(\beta(\omega, t - nb))\right\},\end{aligned} \tag{7}$$

where $\beta(\omega, t - nb) \equiv \alpha(\omega - \omega_0) + i(t - nb)/(2\alpha)$, and $W(z)$ is the complex error function.[14,15] When $t \to \infty$, $2 - \exp(z^2)W(z) \to 2$, the amplitude $\varepsilon_{TL}(\omega, t - nb)$ in Eq. (7) becomes $\varepsilon_{TL}(\omega) = \epsilon e^{-\alpha^2(\omega-\omega_0)^2}$ for each n, and Eq. (6) collapses to Eq. (1) due to Jacobi-Anger expansion [Eq. (2)].

The pulse train energy is given as $E_0 = \int_{-\infty}^{+\infty} dt |\varepsilon_{PM}(t)|^2 = (1/(2\pi)) \int_{-\infty}^{+\infty} d\omega |\varepsilon_{PM}(\omega)|^2$. Hence, the pulse energy is unchanged during phase modifications in the frequency domain [Eq. (1)], $\int_{-\infty}^{+\infty} d\omega |\varepsilon_{PM}(\omega)|^2 = \int_{-\infty}^{+\infty} d\omega |\varepsilon_{TL}(\omega)|^2 = 2\pi E_0$, carried out by varying a, b, and c. Control of $P_{S_2}(t)$ by means of the pulse train phase parameters can be understood as a specific particular case of "absolute control" described in Ref. 16.

B. Pulse train induced dynamics

Hereafter $|\kappa\rangle$ denotes vibrational states belonging to the S_2 electronic state, with the corresponding projection operator $Q = \sum_\kappa |\kappa\rangle\langle\kappa|$. These $|\kappa\rangle$ states are not eigenstates of the full vibronic $S_1 + S_2$ Hamiltonian, and hence are time dependent; they are termed resonances below. The states $|\beta\rangle$ denote the vibrational states belonging to the S_1 electronic state, with $P = \sum_\beta |\beta\rangle\langle\beta|$ being the associated projection operator. The full vibronic $S_1 + S_2$ eigenstates are denoted $|\gamma\rangle$, i.e., $H|\gamma\rangle = E_\gamma|\gamma\rangle$. This gives $\sum_\gamma |\gamma\rangle\langle\gamma| = I = P + Q$ on the $S_1 + S_2$ energy domain.

Excitation from S_0 by a pulse train [Eq. (4)] produces an excited wave packet on $S_1 + S_2$:

$$|\Psi(t)\rangle = \sum_\gamma d_\gamma(t) e^{-iE_\gamma t/\hbar} |\gamma\rangle. \tag{8}$$

If the exciting laser pulse is weak, as in Refs. 2–4, first-order time dependent perturbation theory is valid, in which case, $d_\gamma(t)$ can be written as

$$d_\gamma(t) = (i/\hbar)\langle\gamma|\mu|g\rangle \varepsilon_{PM}(\omega_{\gamma g}, t), \tag{9}$$

where μ is the transition dipole operator, $|g\rangle$ is the ground state on $|S_0\rangle$, and $\omega_{\gamma g} \equiv (E_\gamma - E_g)/\hbar$.

Consider then control over the population in S_2, denoted $P_{S_2}(t)$. The S_2 population is the observable associated with the projector Q in the state $|\Psi(t)\rangle$. In the $|\gamma\rangle$ basis, the Q operator has a $\mathbf{Q}$ matrix with matrix elements composed of $\langle\gamma'|Q|\gamma''\rangle = \sum_\kappa \langle\gamma'|\kappa\rangle\langle\kappa|\gamma''\rangle$. Thus, $\mathbf{Q}$ has the form $\mathbf{Q} = \mathbf{R}\mathbf{R}^\dagger$, where $R_{\gamma,\kappa} = \langle\gamma|\kappa\rangle$. The S_2 population can then be expressed in matrix-vector form as

$$\begin{aligned}P_{S_2}(t) &= \langle\Psi(t)|Q|\Psi(t)\rangle = \mathbf{j}^\dagger \mathbf{E}^\dagger(t) \underline{\underline{\mu}}^\dagger \underline{\underline{\mathbf{e}}}^{iEt/\hbar} \mathbf{R}\mathbf{R}^\dagger \underline{\underline{\mathbf{e}}}^{-iEt/\hbar} \underline{\underline{\mu}} \mathbf{E}(t)\mathbf{j} \\ &= \underline{\varepsilon}^\dagger(t)\mathbf{M}^\dagger(t)\mathbf{M}(t)\underline{\varepsilon}(t) = \underline{\varepsilon}^\dagger(t)\mathbf{K}(t)\underline{\varepsilon}(t).\end{aligned} \tag{10}$$

In Eq. (10) $\underline{\varepsilon}(t)$ is the vector composed of $\varepsilon_{PM}(\omega_{\gamma g}, t)$ values which, due to Eq. (6), can be written as $\underline{\varepsilon}(t) = \mathbf{E}(t)\mathbf{j}$, where $\mathbf{E}(t)$ is the matrix composed of $e^{inb\omega_{\gamma g}} \varepsilon_{TL}(\omega_{\gamma g}, t - nb)$ values (depending on the b parameter), and $\mathbf{j}$ is the vector composed of $J_n(a)e^{inc}$ values (depending on a and c parameters). The $\underline{\underline{\mathbf{e}}}^{\pm iEt/\hbar}$ is a diagonal matrix composed of $e^{\pm iE_\gamma t/\hbar}$, and $\underline{\underline{\mu}}$ is the diagonal matrix composed of $(i/\hbar)\langle\gamma|\mu|g\rangle$. The matrix $\mathbf{M}(t)$,

$$\mathbf{M}(t) = \mathbf{R}^\dagger \underline{\underline{\mathbf{e}}}^{-iEt/\hbar} \underline{\underline{\mu}}, \tag{11}$$

is the material system matrix composed of elements

$$M_{\kappa,\gamma}(t) = \langle\kappa|\gamma\rangle e^{-iE_\gamma t/\hbar} (i/\hbar)\langle\gamma|\mu|g\rangle, \tag{12}$$

while

$$\mathbf{K}(t) \equiv \mathbf{M}^\dagger(t)\mathbf{M}(t) \tag{13}$$

is the full (combined) material system matrix, having matrix elements

$$\begin{aligned}K_{\gamma',\gamma''}(t) &= \sum_\kappa M^*_{\kappa,\gamma'}(t) M_{\kappa,\gamma''}(t) \\ &= \frac{1}{\hbar^2}\langle g|\mu|\gamma'\rangle\langle\gamma''|\mu|g\rangle e^{-i(E_{\gamma''} - E_{\gamma'})t/\hbar} \\ &\quad \times \sum_\kappa \langle\gamma'|\kappa\rangle\langle\kappa|\gamma''\rangle.\end{aligned} \tag{14}$$

Time dependence in Eq. (10) is provided by both $\underline{\underline{\mathbf{e}}}^{\pm iEt/\hbar}$ and $\mathbf{E}(t)$, the latter being time dependent during the action of the pulse train. It is noteworthy that the $\mathbf{M}(t)$ and $\mathbf{K}(t)$ matrices depend only on the material system properties, while the $\underline{\varepsilon}(t) = \mathbf{E}(t)\mathbf{j}$ vector depends only on pulse train properties. Equation (10) can be rewritten in scalar form as a

sum of diagonal (d) and interference (i) parts:

$$P_{S_2}(t) = \sum_{\kappa} \left| \sum_{\gamma} M_{\kappa,\gamma}(t)\, \varepsilon_{PM}(\omega_{\gamma g}, t) \right|^2 = P^{\mathrm{d}}_{S_2}(t) + P^{\mathrm{i}}_{S_2}(t)$$

$$= \sum_{\gamma'} \frac{\epsilon^2}{4} e^{-2\alpha^2(\omega_{\gamma' g}-\omega_0)^2} \left| \sum_{n'=-\infty}^{n'=+\infty} J_{n'}(a) e^{i\, n'(b\,\omega_{\gamma' g}+c)} \left\{ 2 - e^{[\beta(\omega_{\gamma' g}, t-n'b))]^2} W(\beta(\omega_{\gamma' g}, t-n'b)) \right\} \right|^2 K_{\gamma',\gamma'}(t)$$

$$+ \sum_{\gamma' \neq \gamma''} \frac{\epsilon^2}{4} e^{-\alpha^2[(\omega_{\gamma' g}-\omega_0)^2+(\omega_{\gamma'' g}-\omega_0)^2]} \left[\sum_{n'=-\infty}^{n'=+\infty} J_{n'}(a) e^{-i\, n'(b\,\omega_{\gamma' g}+c)} \left\{ 2 - e^{[\beta^*(\omega_{\gamma' g}, t-n'b)]^2} W(-\beta^*(\omega_{\gamma' g}, t-n'b)) \right\} \right]$$

$$\times \left[\sum_{n''=-\infty}^{n''=+\infty} J_{n''}(a) e^{i\, n''(b\,\omega_{\gamma'' g}+c)} \left\{ 2 - e^{[\beta(\omega_{\gamma'' g}, t-n''b)]^2} W(\beta(\omega_{\gamma'' g}, t-n''b)) \right\} \right] K_{\gamma',\gamma''}(t), \tag{15}$$

where the property $W^*(z) = W(-z^*)$ has been used.[15] Both the diagonal and nondiagonal parts of Eq. (15) depend on the phase parameters a, b, and c. When the pulse train is over, the finite-time Fourier transform of the pulse train becomes time independent, and Eq. (15), due to Eq. (2), simplifies to

$$P_{S_2}(t) = \sum_{\kappa} \left| \sum_{\gamma} M_{\kappa,\gamma}(t)\, \varepsilon_{PM}(\omega_{\gamma g}) \right|^2 = P^{\mathrm{d}}_{S_2}(t) + P^{\mathrm{i}}_{S_2}(t) = \sum_{\gamma'} \epsilon^2 e^{-2\alpha^2(\omega_{\gamma' g}-\omega_0)^2} K_{\gamma',\gamma'}(t)$$

$$+ \sum_{\gamma' \neq \gamma''} \epsilon^2 e^{-\alpha^2[(\omega_{\gamma' g}-\omega_0)^2+(\omega_{\gamma'' g}-\omega_0)^2]} e^{i2a\,\sin(b(\omega_{\gamma'' g}-\omega_{\gamma' g})/2)\cos(b(\omega_{\gamma'' g}+\omega_{\gamma' g})/2+c)} K_{\gamma',\gamma''}(t). \tag{16}$$

Equations (15) and (16) give the general description of weak field pulse train induced $S_0 \to S_1 + S_2$ excitation and $S_2 \leftrightarrow S_1$ interconversion dynamics of the closed quantum system in the perturbative regime. Note that phase dependence arises solely from the nondiagonal (interference) part in Eq. (16). Since $\underline{\underline{\mu}}$ and $\underline{\underline{\mathbf{e}}}^{\pm iEt/\hbar}$ are diagonal, the only source of $\mathbf{K}(t)$ nondiagonality in Eqs. (15) and (16) is $\mathbf{Q} = \mathbf{R}\mathbf{R}^{\dagger}$. Thus, control via the phases $\phi_\gamma(t)$ of the complex functions $\varepsilon_{PM}(\omega_{\gamma g}, t)$ depends solely on properties of $\mathbf{Q}$.

Consider then the nature of the $\mathbf{R}$ and $\mathbf{Q}$ matrices. $\mathbf{R}$ is a rectangular matrix with each κth column composed of overlaps $R_{\gamma,\kappa} = \langle\gamma|\kappa\rangle$ of the particular resonance $|\kappa\rangle$ with all available $|\gamma\rangle$ states. Each $|\kappa\rangle$ resonance, being broadened in energy, has more than one nonzero $\langle\gamma|\kappa\rangle$ term in its own column. If resonances $|\kappa\rangle$ and $|\kappa'\rangle$ overlap, then, by definition, they have at least one common $|\gamma\rangle$ state such that for this $|\gamma\rangle$ both $R_{\gamma,\kappa} \neq 0$ and $R_{\gamma,\kappa'} \neq 0$. The corresponding $|\kappa\rangle$th and $|\kappa'\rangle$th columns overlap.

All nonzero $\langle\gamma|\kappa\rangle$ components of each column in $\mathbf{R}$ related to one particular resonance $|\kappa\rangle$ form a square block centered on the main diagonal and filled by terms $Q_{\gamma',\gamma''} = \langle\gamma'|\kappa\rangle\langle\kappa|\gamma''\rangle$ in the resulting $\mathbf{Q} = \mathbf{R}\mathbf{R}^{\dagger}$ matrix. Hence, $\mathbf{Q}$ acquires a block-diagonal structure. Since each block dimensionality is larger than one due to resonance energy broadening, nondiagonal matrix elements in these blocks are generally nonzero, contributing to the $\mathbf{K}(t)$ nondiagonality and thus providing $P_{S_2}(t)$ phase control associated with the energy broadening of each particular resonance. Furthermore, if two resonances $|\kappa\rangle$ and $|\kappa'\rangle$ overlap, then the corresponding blocks overlap so that the $\mathbf{Q}$ matrix acquires a nonblock-diagonal structure. In this case the $Q_{\gamma',\gamma''}$ belonging to two blocks simultaneously are a sum of terms borrowed from each block produced by its corresponding resonance: $Q_{\gamma',\gamma''} = \langle\gamma'|\kappa\rangle\langle\kappa|\gamma''\rangle + \langle\gamma'|\kappa'\rangle\langle\kappa'|\gamma''\rangle$. Similarly, when N blocks overlap, the sum contains N terms: $Q_{\gamma',\gamma''} = \sum_{\kappa=\kappa_1}^{\kappa_N} \langle\gamma'|\kappa\rangle\langle\kappa|\gamma''\rangle$. The effects of resonance broadening and resonance overlap are possible because of the contributions of phase control by means of nondiagonal $P_{S_2}(t)$. Significantly, resonance overlap substantially increases controllability in the presence of the resonance broadening.

We note, similar to Ref. 5, that, since terms in Eq. (15) contain the series over n (different TL bursts in the pulse train), this can provide time based interferences, thus making the transient $P_{S_2}(t)$ behavior more complex. However, this is not the case after the pulse is over [Eq. (16)] because the sum over n collapses to the single term due to Jacobi-Anger expansion [Eq. (2)].

III. NUMERICAL EXAMPLES

This section presents numerical results for 24-mode pyrazine $S_0 \to S_2$ excitation and associated $S_2 \leftrightarrow S_1$ IC dynamics,[6–8] as well as a simple two-dimensional model that qualitatively describes excitation and IC dynamics in β-carotene. Both results show the influence of resonance broadening and resonance overlap on phase controllability, as discussed below. For both systems S_2 population dynamics is computed using Eq. (15) [which becomes Eq. (16) when and after the pulse is over].

A. Pyrazine

Consider first $S_0 \to S_2$ excitation of pyrazine under pulse train action. The pyrazine vibronic structure description is that of Refs. 6–8, which was obtained as a converged iterative solution of the QP-partitioning approach using the Hamiltonian from Ref. 17. The Q space consists of the 176

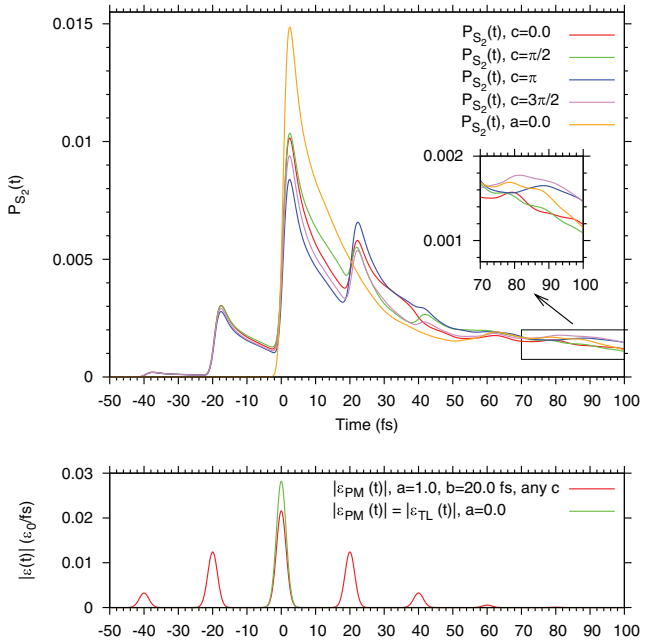

FIG. 1. Upper panel: Pyrazine $P_{S_2}(t)$ populations produced by Gaussian pulse trains with $a = 1.0$, $b = 20.0$ fs, $c = 0.0, \pi/2, \pi, 3\pi/2$, together with $P_{S_2}(t)$ population generated by a Gaussian TL pulse, denoted by $a = 0.0$. Lower panel: Time envelope of the same pulse trains in the units of ϵ_0/fs (see text) together with time envelope of the TL pulse (green). The parameters $\alpha = 1.0$ fs and $E_0 = \hbar\omega_0 = 4.77$ eV in all the cases. Inset shows the residual dynamics after the pulse train is over, magnified for clarity.

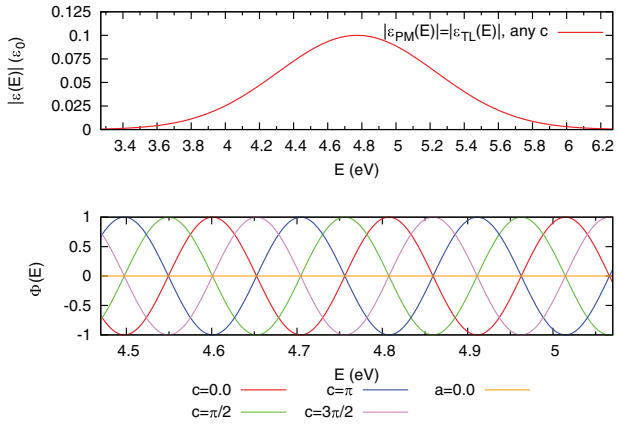

FIG. 2. Upper panel: Amplitude $|\varepsilon_{PM}(E)|$ in the units of ϵ_0 (see text) of Gaussian pulse trains in the frequency (energy) domain with $a = 1.0$, $b = 20.0$ fs, $c = 0.0, \pi/2, \pi, 3\pi/2$, coinciding with the amplitude $|\varepsilon_{TL}(E)|$ of Gaussian TL pulse having $a = 0.0$. Lower panel: Phases $\Phi_{PM}(E)$ of the same pulse trains, together with the phase $\Phi_{TL}(E)$ of the TL pulse ($\Phi_{TL}(E) \equiv 0$). The parameters $\alpha = 1.0$ fs and $E_0 = \hbar\omega_0 = 4.77$ eV in all the cases, and the values of c are shown at the bottom of the figure.

brightest (most optically accessible) $|\kappa\rangle$ resonances, defined as having the largest values of the $|\langle\kappa|\mu|g\rangle|$ transition dipole matrix elements. In this case the *QP*-partitioning approach provided 76 775 "coarse-grained" vibronic states $|\overline{\alpha}\rangle$, used instead of exact vibronic states $|\gamma\rangle$. These coarse-grained states $|\overline{\alpha}\rangle$ are described in detail in Refs. 6–8. This yields 76 775 $\times$ 176 = 13 512 400 values of $R^{\alpha}_{\alpha,\kappa} = \langle\overline{\alpha}|\kappa\rangle$, which are used together with 176 $\langle\kappa|\mu|g\rangle$ values to compute the $P_2(t)$ dynamics within the framework of the doorway states approximation. In this approximation, $\langle\overline{\alpha}|\mu|g\rangle$ is given by $\langle\overline{\alpha}|\mu|g\rangle = \sum_{\kappa}\langle\overline{\alpha}|\kappa\rangle\langle\kappa|\mu|g\rangle$, as discussed in detail in Ref. 8.

Characteristic examples of the $P_{S_2}(t)$ populations produced by pulse trains with different parameters are shown in the upper panel of Fig. 1, together with $P_{S_2}(t)$ population generated by a TL pulse. All pulses have the central frequency corresponding to 4.77 eV in energy, with $\alpha = 1.0$ fs. For the pulse trains, $a = 1.0$ and $b = 20.0$ fs are fixed and chosen so as to obtain a total pulse train duration of $\approx$100 fs, similar to the characteristic internal conversion decay times of $P_{S_2}(t)$, which are in the range 20–100 fs.[6,7] The phase parameter c is then set to $c = 0.0, \pi/2, \pi, 3\pi/2$ to explore phase control over the $P_{S_2}(t)$ population. The populations for all the cases are computed using Eq. (15), where it suffices to truncate the sums over n' and n'' at the same threshold number n_T and perform the n' and n'' sums in the range $[-n_T, +n_T]$ inclusively. Here $n_T = \text{Int}(10 \times a) + 1$, i.e., the integer part of the real value (10 times a) plus one.

Figure 1 (lower panel) shows pulse train envelopes in the time domain together with the envelope of the TL pulse in the units of ϵ_0/fs, where $\epsilon_0 = 1.89 \times 10^{10}$ (V/m) fs. The field amplitude ϵ [see Eq. (1)] is equal to $0.1\epsilon_0 = 1.89 \times 10^9$ (V/m) fs for all the calculations below. As can be seen in Figure 1, the peak magnitude of the electric field amplitude used is equal to $\approx$0.0282 ϵ_0/fs = 5.33 $\times 10^8$ V/m, corresponding to the weak field excitation regime by the femtosecond laser. The nature of the fields in the frequency domain is shown in Figure 2 with the amplitude (upper panel) in ϵ_0 units and phase (lower panel) in the frequency (energy) domain, together with the amplitude and phase of the TL pulse. In the frequency domain, the field amplitude is the same for all the cases, while the pulse train phases follow a simple sinusoidal pattern [see Eq. (1)].

The phase control seen in Fig. 1 (top panel) is to be strong in the transient regime (during the time that the pulse train is acting on the system). However, after the pulse is over, the pulse train phase control over the remaining population is in the 10% to 30% range, qualitatively similar to Ref. 16.

B. Model β-carotene

Experiments on the pulse train control[2–4] of β-carotene dynamics served as one motivation for this study. The absence of reliable potential surfaces for this system motivated a minimal model,[5] which we use below. Specifically, we present numerical examples of perturbative $S_0 \rightarrow S_2$ excitation and $S_2 \leftrightarrow S_1$ IC dynamics for a two-dimensional model with product Morse potential

$$\begin{aligned} V^{2D}_{c,t}(x_c, x_t) &= C_{c,t}\left[E^0_c + D_c(1 - e^{-a_c(x_c - x_{e,c})})\right] \\ &\quad \times \left[E^0_t + D_t(1 - e^{-a_B(x_t - x_{e,t})})\right] \\ &\equiv C_{c,t} V^{1D}_c(x_c) V^{1D}_t(x_t), \end{aligned} \tag{17}$$

where x_c and x_t are the coupling and tuning coordinates (hereafter "c" means "coupling" and "t" means "tuning"), having equilibrium values $x_{e,c}$ and $x_{e,t}$, respectively. The potential $V^{2D}_{c,t}(x_c, x_t)$ for the ground potential energy surface $|S_0\rangle$ is adjusted to existing experimental data (see Ref. 5) giving the parameters $C_{c,t} = 0.9381$ eV^{-1}, $E^0_c = E^0_t = 1.066$ eV ($C_{c,t}E^0_c = C_{c,t}E^0_t = 1.0$), $a_c = 0.5$ a.u.$^{-1}$, $D_c = 0.4$ eV,

μ_c (the effective reduced mass of mode c) = 177.91 a.u., a_t = 1.0 a.u.$^{-1}$, D_t = 0.8 eV, μ_t = 33.69 a.u. These parameters result in a vibronic coupling mode with frequency ω_c and transition energy $\hbar\omega_c = \hbar a_c\sqrt{2C_{c,t}E_t^0 D_c/\mu_c}$ = 178 cm^{-1}, and a tuning mode with frequency ω_t with transition energy $\hbar\omega_t = \hbar a_t\sqrt{2C_{c,t}E_c^0 D_t/\mu_t}$ = 1157 cm^{-1}. The lower frequency mode ω_c is the distortive vibrational mode of β-carotene, similar to that of butadiene,[18] while the latter ω_t is the stretching mode associated with one of the C=C double bonds.[5]

The 2D Hamiltonian $H_{c,t}^{2D}(x_c, x_t) = T_c^{1D}(x_c) + T_t^{1D}(x_t) + V_{c,t}^{2D}(x_c, x_t)$ matrix is constructed in a two mode product basis $|\Phi_{n_c}^c(x_c)\rangle|\Phi_{n_t}^t(x_t)\rangle$ of usual 1D Morse wavefunctions $|\Phi_{n_c}^c(x_c)\rangle$ for the mode x_c and $|\Phi_{n_t}^t(x_t)\rangle$ for the mode x_t (see Ref. 19), making use of analytic matrix elements for the 1D Morse wavefunctions.[19] The choice of 2D potential (17) as a product of 1D potentials allows one to simply express the $H_{c,t}^{2D}$ matrix elements through the one-dimensional T^{1D} and V^{1D} matrix elements for the coupling and tuning modes:

$$\begin{aligned}\left(H_{c,t}^{2D}\right)_{n_c' n_t', n_c'' n_t''} &= \left\langle \Phi_{n_c'}^c(x_c)\middle|\left\langle \Phi_{n_t'}^t(x_t)\middle| H_{c,t}^{2D}(x_c, x_t)\middle|\Phi_{n_c''}^c(x_c)\right\rangle\middle|\Phi_{n_t''}^t(x_t)\right\rangle \\ &= \left(T_c^{1D}\right)_{n_c', n_c''}\delta_{n_t', n_t''} + \left(T_t^{1D}\right)_{n_t', n_t''}\delta_{n_c', n_c''} \\ &\quad + C_{c,t}\left(V_c^{1D}\right)_{n_c', n_c''}\left(V_t^{1D}\right)_{n_t', n_t''}, \end{aligned} \tag{18}$$

where the (tedious) expression for $(T_c^{1D})_{n_c', n_c''}$ and $(T_t^{1D})_{n_t', n_t''}$ is given in Ref. 19,

$$\left(V_c^{1D}\right)_{n_c', n_c''} = E_{n_c'}^{\text{Morse}}\,\delta_{n_c', n_c''} - \left(T_c^{1D}\right)_{n_c', n_c''}, \tag{19}$$

$$E_{n_c'}^{\text{Morse}} = E_c^0 + \hbar a_c\sqrt{\frac{2D_c}{\mu_c}}\left(n_c + \frac{1}{2}\right) - \frac{\hbar^2 a_c^2}{2\mu_c}\left(n_c + \frac{1}{2}\right)^2, \tag{20}$$

and the same formulae hold true for the tuning mode. The set of parameters supports 36 $|\Phi_{n_c}^c(x_c)\rangle$ 1D basis functions for the coupling mode, and 11 $|\Phi_{n_t}^t(x_t)\rangle$ 1D basis functions for the tuning mode, so that the 2D product basis $|\Phi_{n_c}^c(x_c)\rangle|\Phi_{n_t}^t(x_t)\rangle$ consists of 36 × 11 = 396 vibrational basis functions. Diagonalization of the 2D Hamiltonian matrix [Eq. (18)] provides 396 2D vibrational states as the linear combinations of these 2D product basis functions.

Since the shape of the S_1 and S_2 surfaces for the β-carotene is poorly known, we follow Ref. 5, using the same model S_0 potential energy surface shape (described above), but being appropriately shifted to represent the S_1 and S_2 states. To do so, the S_1 and S_2 surfaces are first raised up in energy with respect to S_0: $E_{S_1} - E_{S_0}$ = 0.786 eV, $E_{S_2} - E_{S_0}$ = 2.584 eV. In addition, the equilibrium coordinates for coupling mode and tuning mode for S_1 and S_2 are shifted with respect to these of S_0 as in Ref. 5: $x_{e,c}^{S_1} - x_{e,c}^{S_0}$ = 6.3 a.u., $x_{e,t}^{S_1} - x_{e,t}^{S_0}$ = 1.5 a.u., $x_{e,c}^{S_2} - x_{e,c}^{S_0}$ = 1.5 a.u., $x_{e,t}^{S_2} - x_{e,t}^{S_0}$ = 0.9 a.u. Linear vibronic coupling is assumed between S_1 and S_2, with the strength V_c = 0.045 eV. Since S_1 and S_2 are taken to be identical in shape to S_0, each of S_1 and S_2 on its own also supports 396 vibrational states. A variational solution of the vibronic $S_1 + S_2$ problem in the full vibronic product basis gives 2 × 396 = 792 vibronic states $|\gamma\rangle$, while the 396 S_2-only states are resonances $|\kappa\rangle$ resulting from the nonzero vibronic coupling strength V_c.

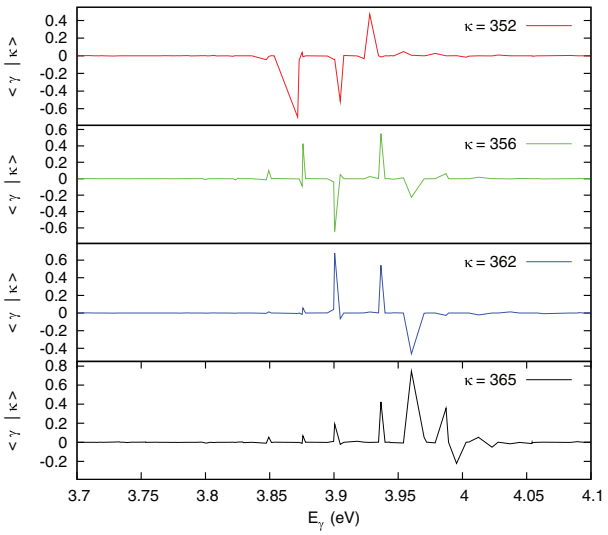

FIG. 3. Four $|\kappa\rangle$ resonances having κ = 352, 356, 362 and 365, presented as their expansion in terms of full vibronic states $|\gamma\rangle$.

Examples of particular $|\kappa\rangle$ resonances obtained in the framework of this model are presented in Fig. 3. Generally, the maxima of the resonances tend to monotonically increase with ascending κ number, although there are some exceptions, *e.g.*, resonances with κ = 356 and 362 have the same maxima. All the resonances remain quite irregular and nonmonotonic in terms of their "shape," which, in our experience, turns out to be a generic feature in behavior of discrete multilevel vibronic problems. Note that the resonances tend to be broad, so that overlap is common.

Due to the low density of states, time evolving populations would have large recurrencies that are unphysical in real polyatomic molecules.[6,7] To correct for this we introduce a simple model to account for population that is lost to other modes. Specifically, we introduce the non-Hermitian Hamiltonian $H = H_0 + H_{\text{abs}}$, where $H_0|\gamma\rangle = E_\gamma|\gamma\rangle$ and $H_{\text{abs}} = -(i/2)\sum_\gamma \Gamma_\gamma|\gamma\rangle\langle\gamma|$, the second term H_{abs} describing the loss of population to background modes. In this case, with the S_0 vibrational ground state $|g\rangle$ optically coupled to the excited $S_2 + S_1$ levels $|\gamma\rangle$, the first-order perturbation theory gives the time dependent wave packet coefficients

$$\widetilde{d}_\gamma(t) = e^{-\Gamma_\gamma t/(2\hbar)}(i/\hbar)\langle\gamma|\mu|g\rangle\varepsilon_{PM}(\mathrm{w}_{\gamma g}, t), \tag{21}$$

where $\mathrm{w}_{\gamma g} \equiv \omega_{\gamma g} - i\Gamma_\gamma/(2\hbar) \equiv (E_\gamma - E_g)/\hbar - i\Gamma_\gamma/(2\hbar)$ are the complex excitation frequencies.

As a result, the material system matrix elements become

$$\begin{aligned}\widetilde{M}_{\kappa,\gamma}(t) &= \langle\kappa|\gamma\rangle e^{-iE_\gamma t/\hbar}e^{-\Gamma_\gamma t/(2\hbar)}(i/\hbar)\langle\gamma|\mu|g\rangle \\ &\equiv \langle\kappa|\gamma\rangle e^{-i\widetilde{E}_\gamma t/\hbar}(i/\hbar)\langle\gamma|\mu|g\rangle, \end{aligned} \tag{22}$$

where complex energies $\widetilde{E}_\gamma \equiv E_\gamma - i\Gamma_\gamma/2$. The $\widetilde{\mathbf{M}}(t)$ matrix can then be written as

$$\widetilde{\mathbf{M}}(t) = \mathbf{R}^\dagger \underline{\underline{\mathbf{e}}}^{-i\widetilde{E}t/\hbar}\underline{\underline{\mu}}, \tag{23}$$

where $\underline{\underline{\mathbf{e}}}^{-i\widetilde{E}t/\hbar}$ is the diagonal matrix composed of $e^{-i\widetilde{E}_\gamma t/\hbar}$ values. As a result,

$$\widetilde{\mathbf{K}}(t) = \widetilde{\mathbf{M}}^\dagger(t)\widetilde{\mathbf{M}}(t) = \underline{\underline{\mu}}^\dagger \underline{\underline{\mathbf{e}}}^{i\widetilde{E}^* t/\hbar}\mathbf{R}\mathbf{R}^\dagger \underline{\underline{\mathbf{e}}}^{-i\widetilde{E}t/\hbar}\underline{\underline{\mu}}, \tag{24}$$

with matrix elements

$$\begin{aligned}\widetilde{K}_{\gamma',\gamma''}(t) &= \sum_\kappa \widetilde{M}^*_{\kappa,\gamma'}(t)\widetilde{M}_{\kappa,\gamma''}(t) \\ &= \frac{1}{\hbar^2}\langle g|\mu|\gamma'\rangle\langle\gamma''|\mu|g\rangle e^{-i(E_{\gamma''}-E_{\gamma'})t/\hbar}e^{-(\Gamma_{\gamma'}+\Gamma_{\gamma''})t/(2\hbar)} \\ &\quad\times \sum_\kappa \langle\gamma'|\kappa\rangle\langle\kappa|\gamma''\rangle. \end{aligned}\tag{25}$$

In addition, to obtain the population in S_2, $\underline{\varepsilon}(t)$ in Eq. (10) is replaced by $\widetilde{\underline{\varepsilon}}(t) = \widetilde{\mathbf{E}}(t)\mathbf{j}$ where the $\widetilde{\mathbf{E}}$ matrix is composed of elements $e^{i\,n\,b\,\mathrm{w}_{\gamma g}}\varepsilon_{TL}(\mathrm{w}_{\gamma g}, t-nb)$. The expression for the resulting population $\widetilde{P}_{S_2}(t)$ is then

$$\begin{aligned}\widetilde{P}_{S_2}(t) &= \langle\widetilde{\Psi}(t)|Q|\widetilde{\Psi}(t)\rangle = \widetilde{\underline{\varepsilon}}^\dagger(t)\widetilde{\mathbf{M}}^\dagger(t)\widetilde{\mathbf{M}}(t)\widetilde{\underline{\varepsilon}}(t) \\ &= \widetilde{\underline{\varepsilon}}^\dagger(t)\widetilde{\mathbf{K}}(t)\widetilde{\underline{\varepsilon}}(t), \end{aligned}\tag{26}$$

where $|\widetilde{\Psi}(t)\rangle$ is an excited wave packet in this case. The expressions for the S_2 population in Eqs. (15) and (16) are changed correspondingly. Resonance broadening and resonance overlap effects continue to be crucial for efficient phase control, exactly as discussed in Subsection II B.

In the case of β-carotene we adopt a population absorption rate in the form of a decay rate $\Gamma = 0.0225$ eV, taken as the same Γ_γ for all $|\gamma\rangle$ states. This particular value of decay rate allows us to successfully model the population decay between the pulse train bursts, obtained in simulations presented in Fig. 6 of Ref. 3. However, this choice does not play any critical role in the subsequent dynamics. Figure 4 (upper panel) shows the population dynamics of resonances with $\kappa \geq 350$ within the current model for the case of using Gaussian TL pulse having $a = 0.0$, as well as the set of different Gaussian pulse trains with $a = 1.23$, $b = 56.0$ fs, and $c = 0.0$, $\pi/2$, π, $3\pi/2$. Here, the parameters a and b for β-carotene are taken explicitly from Ref. 5 in order to compare the resulting dynamics. The truncation value n_T (its definition is given in Subsection III A) for the β-carotene case (for $a = 1.23$) is 13, and so the summation over n' and n'' here is performed from -13 to 13 inclusively.

Figure 4 (lower panel) shows the associated pulse train envelopes in time domain in the units of ϵ_0/fs together with the envelope of the TL pulse. The overall amplitude of the electric field in Fig. 4 is smaller than that in Fig. 1 because the α value is larger here than that in Fig. 1. The amplitude ratio of different pulse bursts and the time separation between these pulse bursts differs from those in Fig. 1 due to differing a and b.

Figure 5 presents the amplitude (upper panel) in ϵ_0 units and phase (lower panel) of the pulse trains in the frequency (energy) domain, together with the amplitude and phase of the TL pulse. As before, amplitude is the same for all cases, and all pulse train phases are sinusoidal [Eq. (1)]. In the intermediate time range, Fig. 4 for β-carotene is qualitatively similar to Fig. 1, so, in the intermediate regime, usage of a uniform

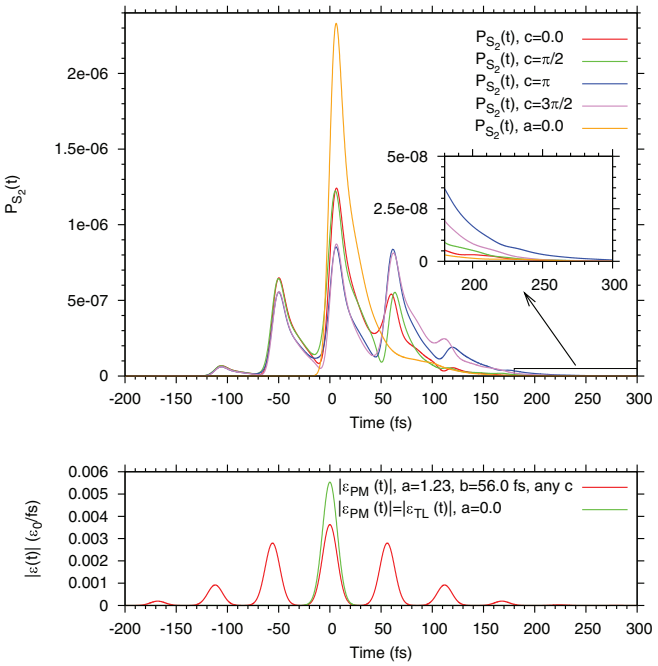

FIG. 4. Upper panel: Model β-carotene $P_{S_2}(t)$ populations, produced by Gaussian pulse trains with $a = 1.23$, $b = 56.0$ fs, $c = 0.0$, $\pi/2$, π, $3\pi/2$, together with $P_{S_2}(t)$ population generated by Gaussian TL pulse having $a = 0.0$. Lower panel: Time envelope of the same pulse trains in the units of ϵ_0/fs (see text) together with time envelope of TL pulse. The parameters $\alpha = 5.1$ fs and $E_0 = \hbar\omega_0 = 3.77$ eV in all the cases. Inset shows the residual dynamics after the pulse train is over, magnified for clarity.

Γ rate proves to be acceptable. As in the case of pyrazine (Fig. 1), phase control is clearly observable in Fig. 4.

The control results for the β-carotene model (Fig. 4) agree qualitatively with the simulated control results for the excited population dynamics in Ref. 3 (see Fig. 6). Namely, the population dynamics is phase-controllable in both the transient regime while the pulse is acting, and in final regime when the pulse is over, i.e., $t > 180$ ps. Note that unlike the discussion in Ref. 3, one does not require an open system to attain this type of one-photon phase control. That is, the

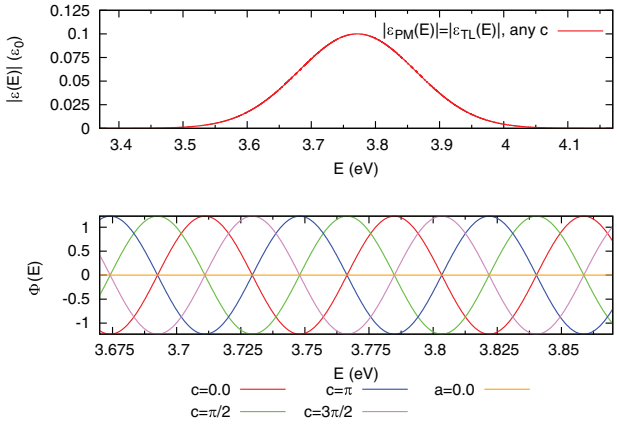

FIG. 5. Upper panel: Amplitude $|\varepsilon_{PM}(E)|$ in the units of ϵ_0 (see text) of Gaussian pulse trains in frequency (energy) domain with $a = 1.23$, $b = 56.0$ fs, $c = 0.0$, $\pi/2$, π, $3\pi/2$, coinciding with the amplitude $|\varepsilon_{TL}(E)|$ of Gaussian TL pulse having $a = 0.0$. Lower panel: Phases $\Phi_{PM}(E)$ of the same pulse trains, together with the phase $\Phi_{TL}(E)$ of the TL pulse ($\Phi_{TL}(E) \equiv 0$). The parameters $\alpha = 5.1$ fs and $E_0 = \hbar\omega_0 = 3.77$ eV in all the cases, and the values of c are shown at the bottom of the figure.

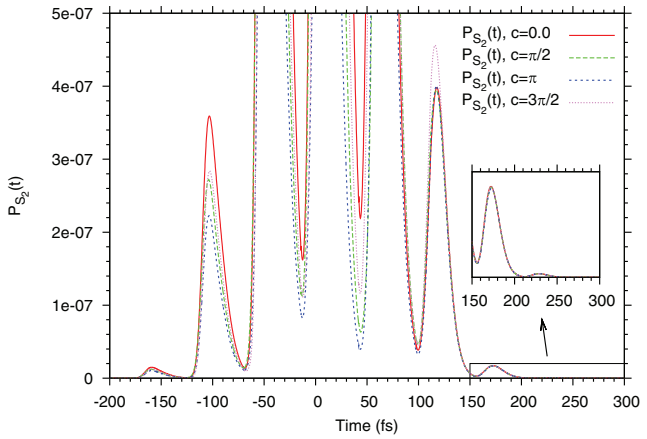

FIG. 6. Model β-carotene $P_{S_2}(t)$ populations, produced by Gaussian pulse trains with $a = 1.23$, $b = 56.0$ fs, $c = 0.0, \pi/2, \pi, 3\pi/2$ for the case of zero $S_1 \leftrightarrow S_2$ coupling ($V_c = 0.0$ eV), meaning no resonance broadening and no resonance overlap. Inset shows the residual dynamics after the pulse train is over, magnified for clarity.

theoretical framework described above, and associated computational results for a closed quantum system, clearly shows this type of phase control in closed systems. This is the case because the observable, the projection operator $Q = \sum_\kappa |\kappa\rangle\langle\kappa|$ representing the S_2 population P_{S_2}, does not commute with the full system Hamiltonian H, thus allowing one-photon phase control.[9]

To clearly show the influence of resonance broadening and resonance overlap on phase control, consider the dynamics of the same β-carotene model system, but (artificially) with zero vibronic $S_1 \leftrightarrow S_2$ coupling ($V_c = 0.0$ eV). In this case each $|\kappa\rangle$ is no longer a resonance, but becomes an eigenstate $|\gamma\rangle$ with zero energy broadening. No resonance overlap takes place in the system. Hence, all nondiagonal $K_{\gamma',\gamma''}(t) = 0$ at any time t in Eq. (15) for the transient regime and Eq. (16) for the final regime, and only the diagonal components in Eqs. (15) and (16) survive. Results for this case are shown in Fig. 6, where different S_2 populations are driven by the same pulse trains as in Fig. 4. As can be seen, different pulse train phase is reflected in the transient dynamics according to the diagonal part of Eq. (15), but at times $t \approx 120$–130 fs, near the end of the pulses, all S_2 populations become indistinguishable, that is, in accord with the diagonal part of Eq. (16), there is no dependence on the pulse phase. Clearly, resonance broadening and resonance overlap are necessary for phase control after the pulse train is over.

IV. SUMMARY AND CONCLUSION

In summary, we have provided an analytical treatment of excited state internal conversion dynamics driven by a Gaussian phase-modulated pulse train in the perturbative regime, and applicable to current experiments. The possibility of coherent control of the population has been analyzed from the point of view of specific material system properties, resonance broadening, and resonance overlap. Two numerical examples of this type of control have been provided, one for Hermitian (pyrazine) and one for non-Hermitian (β-carotene model) cases. Both the computational and analytical results show that resonance broadening and resonance overlap are required to obtain phase control of the population after the pulse train is over. However, resonance broadening and resonance overlap effects have been found to be important as well for excited state transient population dynamics. Specifically, the relative significance of these two effects can be readily summarized: resonance broadening is necessary for phase dependent pulse train control, but the control is greatly enhanced by resonance overlap. Thus these results provide new useful insights into "coherent control spectroscopy," experimentally introduced in Refs. 2–4.

ACKNOWLEDGMENTS

This work was supported by the Natural Sciences and Engineering Research Council of Canada (NSERC) under Grant No. RGPIN 14-10.

[1] M. Shapiro and P. Brumer, *Principles of the Quantum Control of Molecular Processes* (Wiley, New York, 2003); M. Shapiro and P. Brumer, *Quantum Control of Molecular Processes* (Wiley-VCH, Weinheim, 2012).
[2] T. Buckup, J. Hauer, C. Serrat, and M. Motzkus, J. Phys. B: At. Mol. Opt. Phys. **41**, 074024 (2008).
[3] T. Buckup, J. Hauer, J. Voll, R. Vivie-Riedle, and M. Motzkus, Faraday Discuss. **153**, 213 (2011).
[4] J. Möhring, T. Buckup, and M. Motzkus, IEEE J. Sel. Top. Quantum Electron. **18**, 449 (2012).
[5] J. Voll and R. de Vivie-Riedle, New J. Phys. **11**, 105036 (2009); J. Voll, "Quanten-Kontroll-Spektroskopie photochemischer Prozesse in biologischen Modellsystemen," Ph.D. thesis (Ludwig-Maximilians Universität München, 2010); J. Voll, private communication (2012).
[6] P. S. Christopher, M. Shapiro, and P. Brumer, J. Chem. Phys. **124**, 184107 (2006).
[7] P. S. Christopher, M. Shapiro, and P. Brumer, J. Chem. Phys. **125**, 124310 (2006).
[8] T. Grinev, M. Shapiro, and P. Brumer, "Coherent quantum control of $S_2 \leftrightarrow S_1$ internal conversion in pyrazine by means of $S_0 \rightarrow S_2/S_1$ weak field excitation," J. Chem. Phys. (to be published); J. Chem. Phys. **137**, 094302 (2012).
[9] L. A. Pachon, L. Yu, and P. Brumer, Faraday Discuss. **163**, 485 (2013); L. A. Pachon and P. Brumer, J. Chem. Phys. **139**, 164123 (2013); M. Spanner, C. A. Arango, and P. Brumer, *ibid.* **133**, 151101 (2010).
[10] Jacobi-Anger expansion in the form $e^{iz\cos(\theta)} = \sum_{n=-\infty}^{n=+\infty} i^n J_n(z) e^{in\theta}$ is presented in E. W. Weisstein, "Jacobi-Anger Expansion," from MathWorld–A Wolfram Web Resource, http://mathworld.wolfram.com/Jacobi-AngerExpansion.html, while here it was rewritten in the form $e^{iz\sin(\theta)} = \sum_{n=-\infty}^{n=+\infty} J_n(z) e^{in\theta}$, where real a is used as z, and $b\,\omega + c$ is used as θ.
[11] E. W. Weisstein, "Bessel Function of the First Kind," from MathWorld–A Wolfram Web Resource, see http://mathworld.wolfram.com/BesselFunctionoftheFirstKind.html.
[12] M. Shapiro, J. Phys. Chem. **97**(29), 7396 (1993).
[13] M. Shapiro, in *Femtosecond Chemistry*, edited by J. Manz and L. Wöste, (VCH, Weinheim, 1995), p. 321.
[14] E. W. Weisstein, Erf(z) error function, from MathWorld–A Wolfram Web Resource, see http://mathworld.wolfram.com/Erf.html.
[15] M. Abramowitz and I. A. Stegun, *Handbook of Mathematical Functions* (Dover, New York, 1965); Eqs. 7.1.3 and 7.1.8.
[16] T. Grinev, M. Shapiro, and P. Brumer, J. Chem. Phys. **138**, 044306 (2013).
[17] A. Raab, G. A. Worth, H.-D. Meyer, and L. S. Cederbaum, J. Chem. Phys. **110**, 936 (1999).
[18] R. P. Krawczyk, K. Malsch, G. Hohlneicher, R. C. Gillen, and W. Domcke, Chem. Phys. Lett. **320**, 535 (2000), see $\nu_8^{b_u}$.
[19] E. M. Greenawalt and A. S. Dickinson, J. Mol. Spectrosc. **30**, 427 (1969), (Eq. (6)). Please note that Eq. (6) in Ref. 19 contains errors: (i) Overall phase factor should not be $(-1)^{n+m}$, but $\delta_{n,m} + (1-\delta_{n,m})(-1)^{n+m+1}$. (ii) Factor of 1/2 should be before $(2n+1)\delta_{n,m}$ in the third row of Eq. (6) in Ref. 19.